

Supporting Information

Janus Upconverting Nanoplatfom with biodegradability for Glutathione depletion, Near-infrared light induced Photodynamic therapy and an accelerated excretion

Hang Zhou^{a†}, Qunying Li^{a†}, Xi Cheng^b, Chao Zhang^a, Jiawei Sun^c, Linyao Du^d, Jing Cao^a, Yajing Liu^a, Pintong Huang^{a*}

^a Department of Ultrasound, The Second Affiliated Hospital, Zhejiang University School of Medicine, Hangzhou 310000, China.

^b Department of General Surgery, Ruijin Hospital, Shanghai Jiao Tong University School of Medicine, Shanghai, 200025, China.

^c Department of In-patient Ultrasound, The Second Affiliated Hospital of Harbin Medical University, Harbin 150001, China.

^d Department of Ultrasound, The First Affiliated Hospital of Dalian Medical University, Dalian 116011, China.

† contributed equally to this manuscript.

* Corresponding Author.

E-mail addresses: huangpintong@zju.edu.cn (P. Huang)

Reagents

Most of the chemicals were obtained from Sigma-Aldrich Inc (St. Louis, MO). Dulbecco's modified Eagle medium-high glucose (DMEM-HG), RPMI-1640 medium and fetal bovine serum (FBS) were obtained from GIBCO. The kits for phosphocreatine kinase (CK), and creatinine (CRE), alkaline phosphatase (ALB), alanine aminotransferase (ALT), aspartate aminotransferase (AST), blood urea nitrogen (BUN), were purchased from Nanjing Jiancheng Bioengineering Institute (Jiangsu, China).

Characterization

The morphology of nanoparticles was characterized by a transmission electron microscope (JEOL, Ltd., Tokyo, Japan). The size of nanoparticles was measured by a Nano-ZS 90 Nanosizer (Malvern Instruments Ltd., Malvern, UK). The N₂ adsorption-desorption isotherms were measured at 77 K by the Brunauer-Emmett-Teller (BET) method.

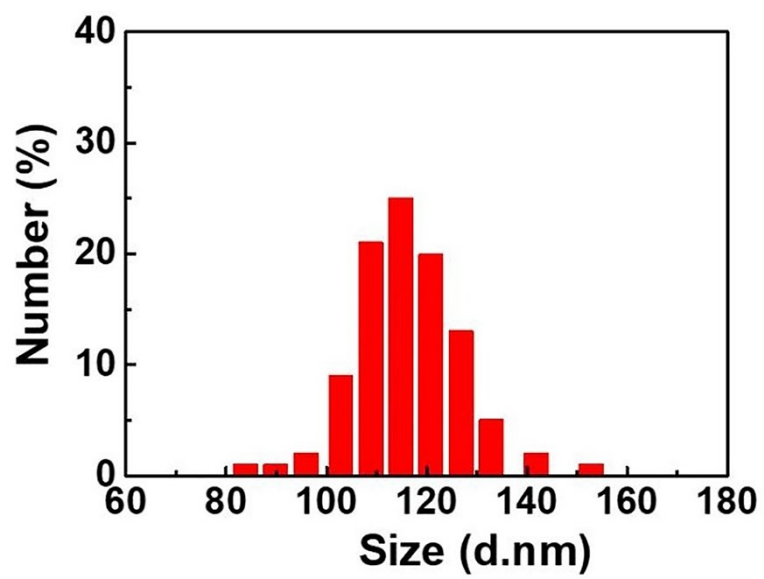


Figure S1. Size distribution of UCN/MONs in water.

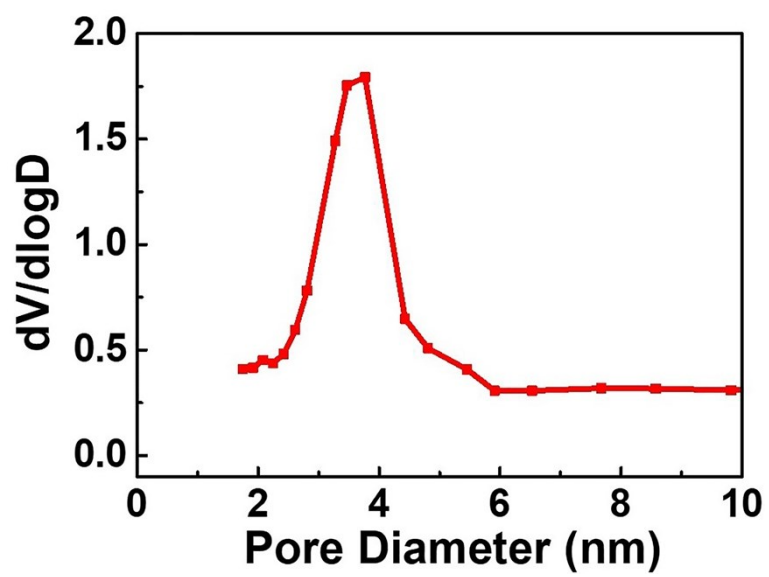


Figure S2. Pore size distribution of UCN/MONs.

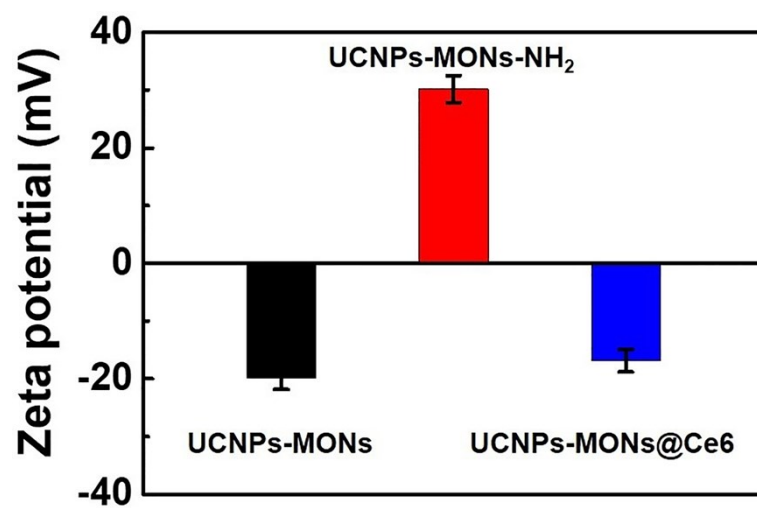


Figure S3. Zeta-potential of UCN/MONs, UCN/MONs-NH₂ and UCN/MONs@Ce6.

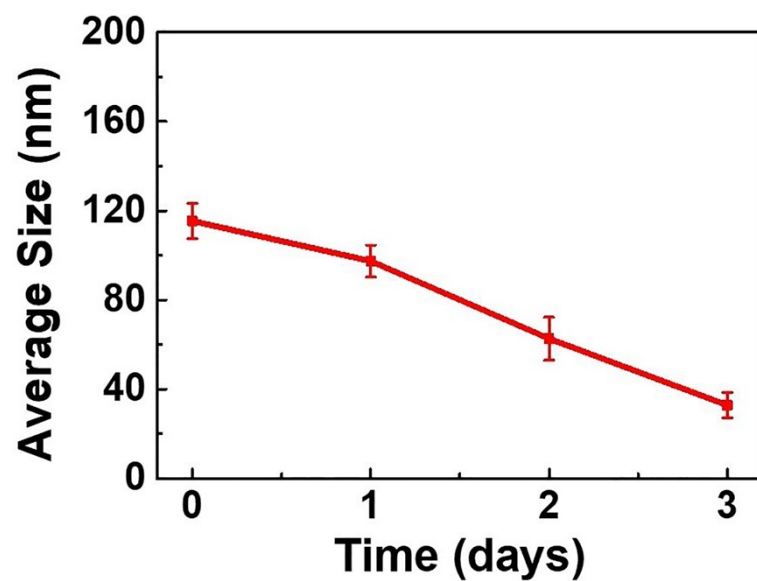


Figure S4. The average size of UCN/MONs after immersed in a 5×10^{-3} m GSH solution for 1, 2 and 3 day.

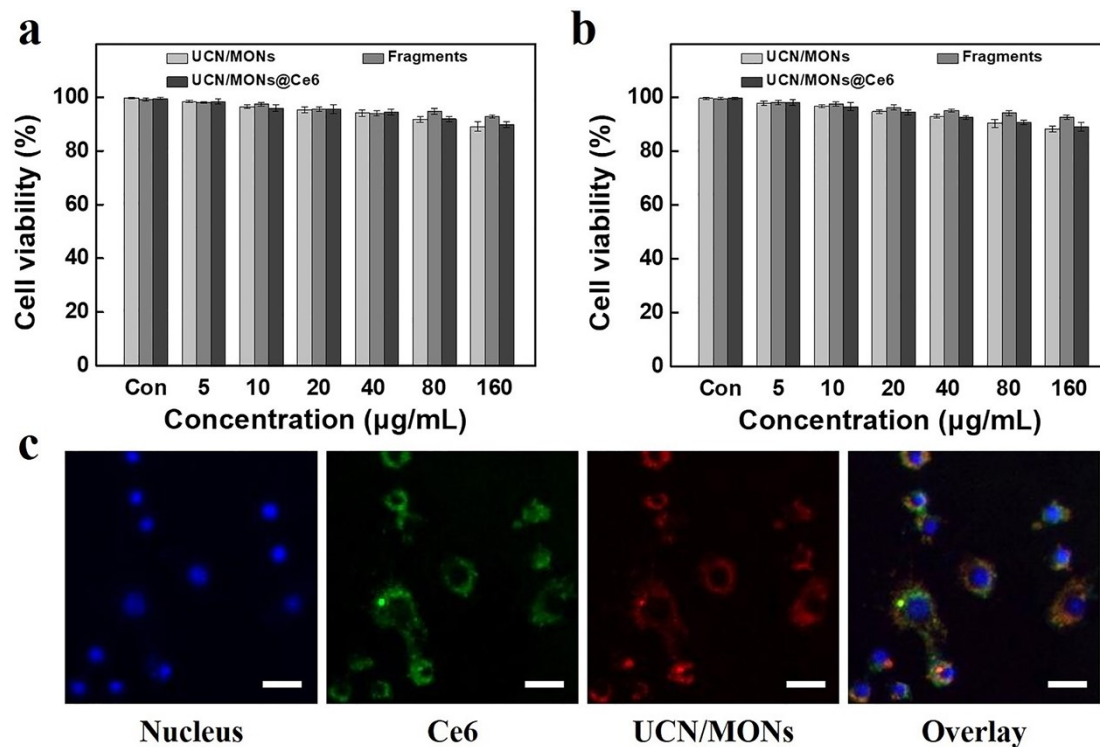


Figure S5. The cytotoxicity of UCN/MONs, UCN/MONs@Ce6 and the degraded UCN/MONs towards (a) MCF-7 cells and (b) MCF 10 A cells after 24 h incubation, n = 5. (c) Confocal microscopy images of MCF-7 cells after 6 h of incubation with UCN/MONs@Ce6. Bar =10 µm.

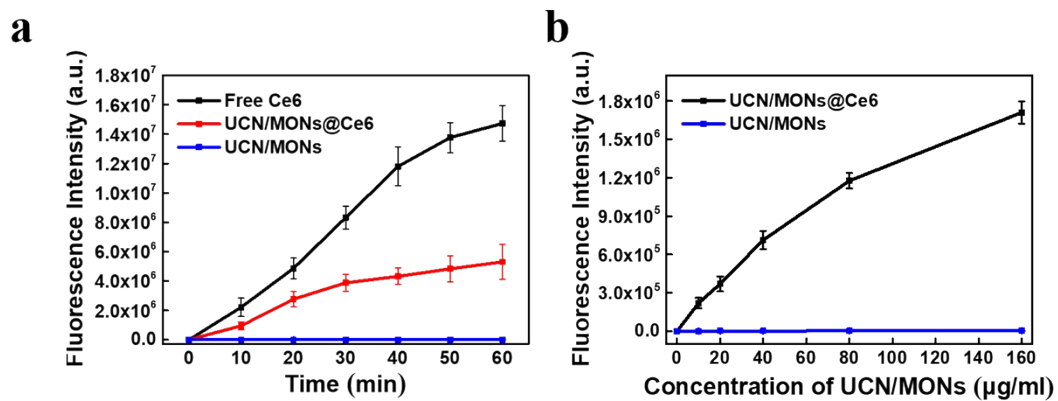


Figure S6. (a) SO generation at various time with the 660 nm laser irradiation. Data represent the mean \pm s.d (n=3). (b) SO generation by various concentration of samples with the 980 nm laser irradiation. Data represent the mean \pm s.d (n = 3).

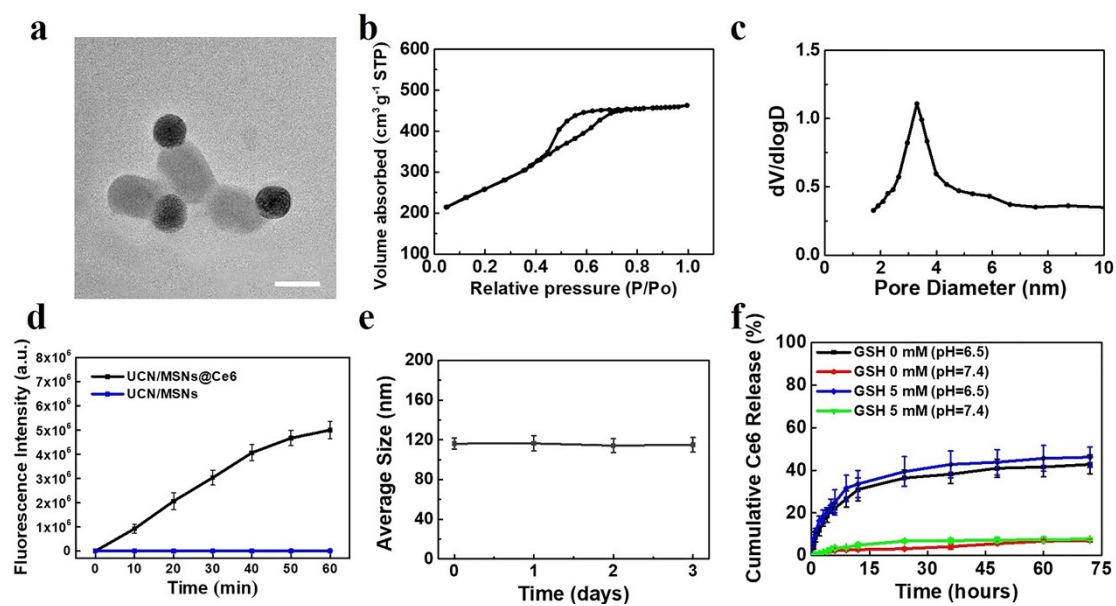


Figure S7. Characterization of UCN/MSNs. (a) TEM. (b) N₂ adsorption-desorption isotherms. (c) The pore size distribution. (d) SO generation at various time with the 980 nm laser irradiation (n = 3). (e) The average size after immersed in a 5×10^{-3} m GSH solution for 1, 2 and 3 day. (f) The Ce6 release behavior in 0 and 5×10^{-3} m GSH (pH = 7.4 and 5.5).

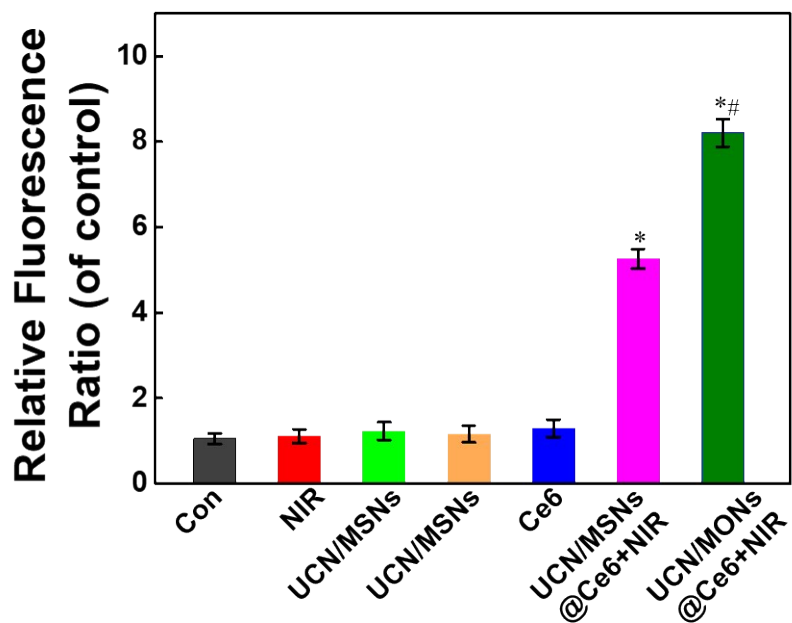


Figure S8. The intracellular ROS fluorescence intensity was determined by FACS after 6 h of exposure. * $p < 0.05$ versus the control group; # $p < 0.05$ versus the UCN/MSNs@Ce6+NIR group.

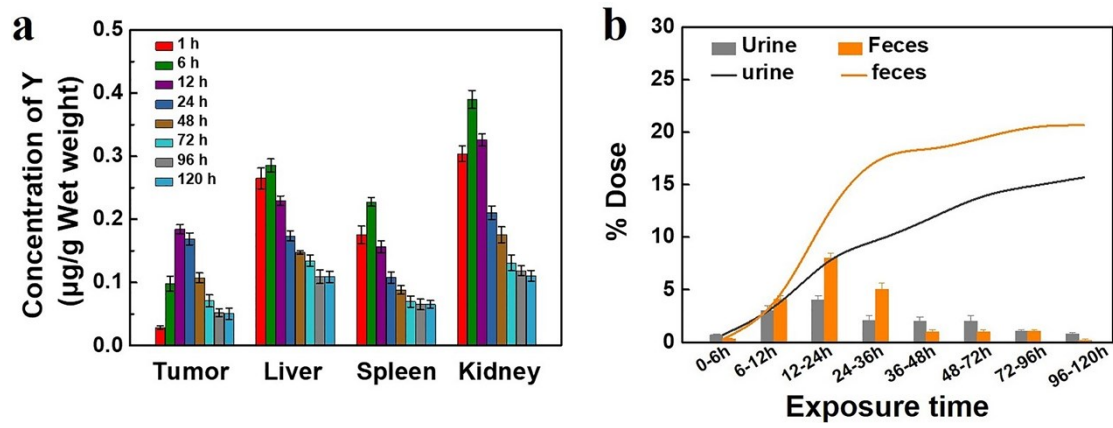


Figure S9. ICP-MS assay of the Clearance of UCN/MSNs@Ce6 in the body. (a) The distribution of Y in tumor, liver, spleen, lung and kidney at various time. (b) Excretion of nanoparticles by urine feces from 0-120 h. All the data represented the mean \pm s.d (n = 5).